Available online at www.sciencedirect.com
SCIENCE DIRECT®
Journal of Power Sources 143 (2005) 227–230
JOURNAL OF POWER SOURCES
www.elsevier.com/locate/jpowsour

Short communication

# The $Ni_3Sn_4$ intermetallic as a novel electrode in lithium cells

I. Amadei[a,*], S. Panero[a], B. Scrosati[a], G. Cocco[b], L. Schiffini[b]

[a] *Department of Chemistry, University of Rome "La Sapienza", 00185 Roma, Italy*
[b] *Department of Chemistry, University of Sassari, 07100 Sassari, Italy*

Received 20 October 2004; accepted 16 November 2004
Available online 23 February 2005

**Abstract**

A $Ni_3Sn_4$ intermetallic compound has been prepared and tested as a new type of anode material. The results show that this compound may be cycled in a lithium cell with a reversible capacity of about 250 mAh $g^{-1}$. This feature, combined with the low cost and the compatibility with the environment, makes $Ni_3Sn_4$ a material of interest for practical applications.


*Keywords:* $Ni_3Sn_4$; Lithium cell; Intermetallic compounds

## 1. Introduction

Great attention has been recently addressed to the development of materials suitable to be used as new types of electrodes in lithium ion batteries. The main goal is to replace the conventional graphite anode and lithium cobalt oxide cathode in view of achieving higher capacity content, lower cost and better environmental compatible compounds [1].

At the anode side, metal storage alloys and intermetallics, are considered among the most promising choices [2–4]. Indeed, large research efforts are presently devoted to this class of materials and many types of them have been prepared and characterized [5–10]. Along this line, we report here the synthesis and the electrochemical properties of a new type of intermetallic compound having the $Ni_3Sn_4$ composition.

## 2. Experimental

### 2.1. Synthesis

$Ni_3Sn_4$ alloy powders were prepared using a commercial high-energy ball mill (Spex Mixer-Mill Model 8000) with stainless-steel balls and vials. The elemental powders of nickel and tin were charged in an argon-filled glove box and the milling was stopped every hour to allow the cooling of the powders into the vials. At regular intervals, a small quantity of powder was taken for XRD analysis.

### 2.2. Electrochemical characterization

For the electrochemical tests, $Ni_3Sn_4$ composite electrodes were prepared by blending 82 wt.% alloy powder (active material), 10% carbon black (Super P as conductive additive), and 8% poly(vinylidene fluoride) (PVdF), (Solvay Solef® 6020 binder). The electrodes were housed in a polypropylene T-type cells, having Li counter and reference electrodes, 1 M $LiClO_4$/ethylene carbonate (EC)–propylene carbonate (PC) (1:1, w/w) electrolyte (Merck Selectipur®), and borosilicate glass–fiber discs (Whatman) as separator. Both electrode fabrication and cell assembly were performed in Ar atmosphere controlled dry box.

The cells, which had an electrode area of 0.785 $cm^2$, were cycled galvanostatically at 0.5 mA $cm^{-2}$ between 20 and 1200 mV versus lithium by a Maccor, series 4000 battery cycler. Cyclic voltammograms have been run, using a VMP Multi-Potentiostat between 1500 and 20 mV with a scan rate of 0.1 mV $s^{-1}$.

* Corresponding author.

0378-7753/$ – see front matter © 2004 Published by Elsevier B.V.
doi:10.1016/j.jpowsour.2004.11.050

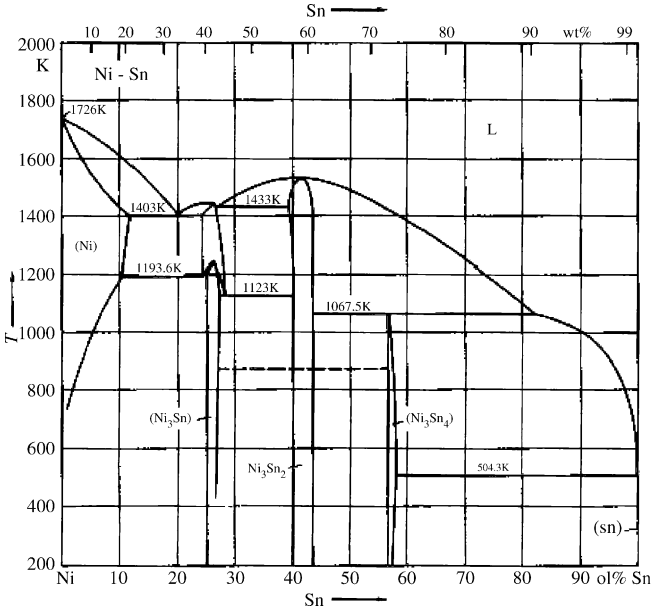


Fig. 1. Ni–Sn phase diagram (derived from reference [11]).

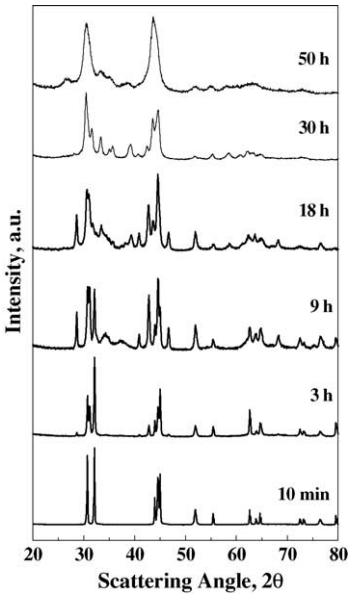


Fig. 2. XRD pattern sequence. The time marks the progressive milling steps in the course of the $Ni_3Sn_4$ synthesis process.

The impedance spectra were recorded in a frequency range between 50 kHz and 10 mHz with an amplitude of 5 mV after the first galvanostatic discharge ($I = 0.03$ mA cm$^{-2}$) and after 100 cycles between 20 and 1500 mV, using a Solartron 1255 HF Frequency Response Analyzer.

## 3. Results and discussion

Fig. 1 shows the Ni–Sn phase diagram [11]. It may be noticed that $Ni_3Sn_4$ is the phase having the highest Sn relative content and that this phase is characterized by a very narrow stability range.

As described in the experimental section, the $Ni_3Sn_4$ compound was prepared by mechanical alloying, by a synthesis process proceeding via subsequent milling steps. Fig. 2 shows the X-ray diffraction patterns of the product of the synthesis, detected at various, progressive milling times. The patterns show that the desired $Ni_3Sn_4$ phase is obtained after 50 h of milling.

Fig. 3 shows an expanded view of the XRD of the final sample and the comparison with the standards reveals that the sample consists of $Ni_3Sn_4$ with contains traces of $SnO_2$.

The final $Ni_3Sn_4$ powder sample was further ground in a agate mortar in the dry box and finally sieved with a 50 μm molecular sieve. Fig. 4 shows a scanning electron microscope (SEM) picture of the sieved sample. Although not totally homogeneous due to the presence of aggregates, the overall morphology may be described as basically formed by particles of average 200 nm size.

It is assumed that the electrochemical process of $Ni_3Sn_4$ in a lithium cell proceeds with a first cathodic step, involving

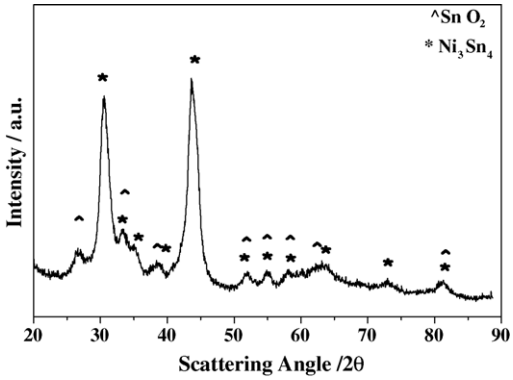


Fig. 3. XRD pattern after 50 h milling.

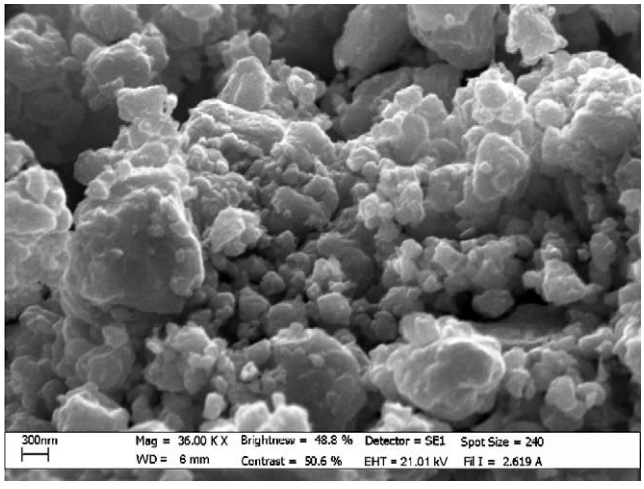


Fig. 4. SEM micrograph of a $Ni_3Sn_4$ alloy sieved powder sample.

the formation of the $Li_{4.4}Sn$ alloy with the separation of Ni:

$$Ni_3Sn_4 + 17.6Li^+ + 17.6e^- \rightarrow 4Li_{4.4}Sn + 3Ni \quad (1)$$

This "activation process" is then followed by the anodic and cathodic reversible electrode process:

$$Li_{4.4}Sn \Leftrightarrow Sn + 4.4Li^+ + 4.4e^- \quad (2)$$

to which is associated a theoretical specific capacity of 725 mAh $g^{-1}$.

Fig. 5 shows a cyclic voltammetry of the $Ni_3Sn_4$ electrode in a three-electrode cell having a Li counter and a Li reference. One may notice the difference between the first and the following cycles. Indeed, in accordance with the mechanism above proposed, the first cathodic scan reveals a peak at about 0.7 V versus Li. This peak is irreversible and probably associated to a combination of processes which may include the activation reaction (1), as well as solvent decomposition, with the formation of a passivating film on the electrode surface [12]. The first cathodic peak is then followed by a second one centered at about 0.26 V versus Li. This peak is reflected by two peaks in the following anodic scan. All the subsequent cycles are reproducible, and thus, representative of the reversible electrode process, see reaction (2). It is difficult to rationalize the splitting of the anodic peak. We may speculate that the lithium–tin alloying process can proceed along two steps characterized by two different energy bands. This is reflected by the two-peak behaviour observed in the anodic scan. On the other hand, only one peak is shown in the cathodic scan; one may assume that this peak is effectively the convolution of the two peaks representing the two-step process. However, a valid interpretation requires further study, also because the suggested two-step behavior is not observed in the galvanostatic alloying–de-alloying curves of the $Ni_3Sn_4$ electrode (see below).

Fig. 6 shows the voltage profile of the $Ni_3Sn_4$ electrode displayed upon cycling in a lithium cell. The first discharge (lithium alloying) curve shows a shoulder around 0.7 V. The subsequent charge (lithium de-alloying) and discharge curves are shown in sequence. Three main aspects are evidenced. First, the 0.7 V shoulder observed at the first cycle is not reproduced in the following cycles, this matching the CV behavior and finally confirming that this voltage is associated to initial irreversible processes. Second, the capacity associated with the reversible cycles is about 40% less than that associated with the first cycle; this initial decay in capacity is also consistent with the above-discussed mechanism since it accounts for both the irreversible activation and the film formation processes. Finally, the two-step behavior observed in the CV curves is not here reproduced in the corresponding charging curves. As already stressed, this poses some difficulties for the full understanding of the mechanism of the electrochemical process.

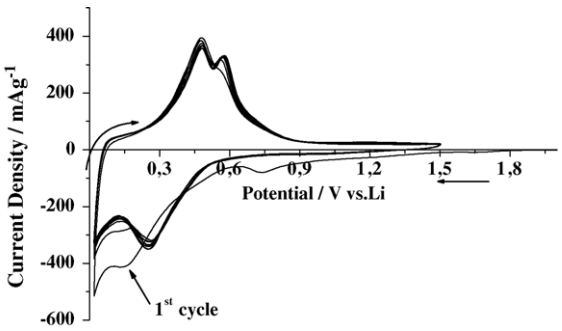


Fig. 5. Cyclic voltammetry of composite $Ni_3Sn_4$ electrodes, recorded between 20 and 1500 mV voltage range with a scan rate of 0.1 mV $s^{-1}$.

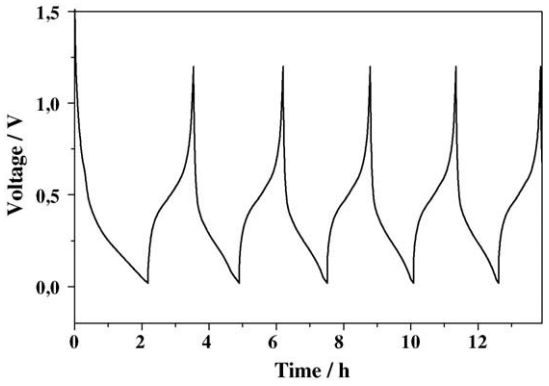


Fig. 6. Electrochemical voltage profile of the Li/$Ni_3Sn_4$ cell, cycled between 1.2 and 0.02 V at 0.5 mA $cm^{-2}$.

Fig. 7 shows the capacity delivered by the $Ni_3Sn_4$ electrode upon cycling in a lithium cell. After the initial loss already discussed, the electrode provides a reversible capacity which averages around 250 mAh $g^{-1}$ with a fade limited to about 0.3% per cycle. This capacity decay upon cycling is probably associated to a progressive increase of the impedance of the intermetallic electrode. This in turn is assumed to be related to two factors, i.e. (i) a slow charge-transfer kinetics and (ii) an interfacial passivation.

Fig. 8a shows the complex impedance response of the electrode after the first discharge cycle. A middle frequency semicircle, representative of the charge-transfer resistance ($R_{ct}$ about 118 ohm), followed by a straight line, representative of the mass diffusion kinetics, are displayed. Fig. 8b

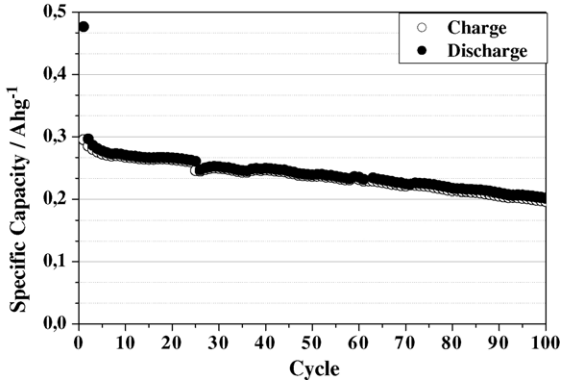


Fig. 7. Specific capacity vs. cycle number for the Li/$Ni_3Sn_4$ cell.

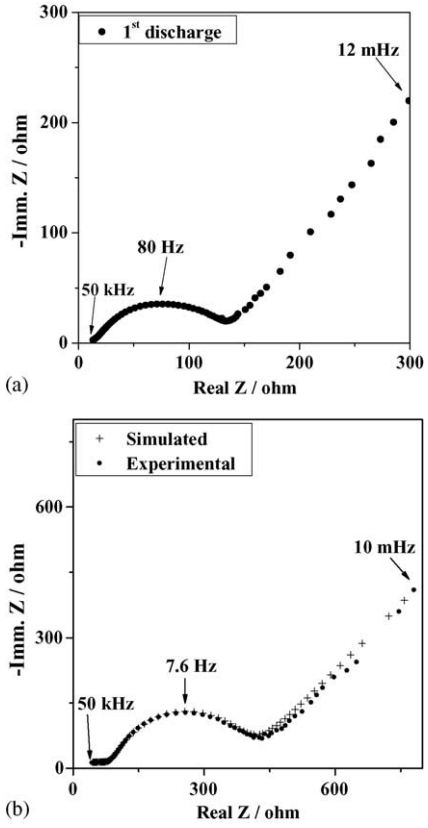


Fig. 8. Experimental and simulated impedance spectra, recorded between 10 mHz and 50 kHz, of the $Ni_3Sn_4$ electrode after the first discharge (a) and after the 100th cycle (b).

shows the response of the same electrode after 100 cycles. The middle frequency semicircle has expanded, revealing an increase of the charge-transfer resistance to a value of about 308 ohm. In addition, a semicircle is evidenced at high frequency, this revealing the formation of a passivating layer on the electrode surface.

It is expected that the kinetics of the intermetallic electrode can be substantially improved by optimizing its morphology, especially in terms of reduction of the particle size. This strategy is under test in our laboratory and the results will be reported in a subsequent paper.

## Acknowledgement

This work has been carried out within the financial support of the Italian Ministry of University and Research MIUR, Project Cofin 2002, “Nanostructured electrode and electrolyte materials for advanced lithium batteries”.

## References

[1] J.L. Tirado, Mater. Sci. Eng. R 40 (2003) 103–136.
[2] R. Huggins, J. Power Sources 26 (1989) 109–120.
[3] R.A. Huggins, Lithium alloy anodes, in: J.O. Besenhard (Ed.), Handbook of Battery Materials, Wiley, New York, 1999.
[4] M. Wachtler, M. Winter, J.O. Besenhard, J. Power Sources 105 (2002) 151–160.
[5] W. Martin, J.O. Besenhard, Electcochim. Acta 45 (1999) 31–50.
[6] J. Yang, Y. Takeda, N. Imanischi, J.Y. Xie, O. Yamamoto, Solid State Ionics 133 (2000) 189–194.
[7] D. Larcher, L.Y. Beaulieu, O. Mao, A.E. George, J.R. Dahn, J. Electrochem. Soc. 147 (2000) 1703–1708.
[8] R. Benedek, M.M. Thackeray, J. Power Sources 110 (2002) 406–411.
[9] C.S. Johnson, J.T. Vaughey, M.M. Thackeray, T. Sarakonsri, S.A. Hackney, L. Fransson, K. Edström, J.O. Thomas, Electrochem. Commun. 2 (2002) 595–600.
[10] M. Wachtler, L. Schiffini, I. Amadei, J. Serra Moreno, S. Bruno, G. Cocco, J. Metastable Nanocrystalline Mater. 20–21 (2004) 263–268.
[11] B. Predel, Phase Equilibria, Crystallographic and Thermodynamic Data of Binary Alloys, Landolt–Börnstein New Series IV/5I, Ed. Springer, pp. 34–36.
[12] E. Peled, D. Golodnitsky, J. Pencier, in: J.O. Besenhard (Ed.), Handbook of Battery Materials, Wiley, New York, 1999, p. 419.